frontiers in Astronomy and Space Sciences

ORIGINAL RESEARCH
published: 26 August 2021
doi: 10.3389/fspas.2021.676281

# Small Mirrors for Small Satellites: Design of the Deformable Mirror Demonstration Mission CubeSat (DeMi) Payload

*Ewan S. Douglas[1,2]*, Greg Allan[2], Rachel Morgan[2], Bobby G. Holden[2], Jennifer Gubner[2], Christian Haughwout[2], Paula do Vale Pereira[2], Yinzi Xin[2,3], John Merk[4] and Kerri L. Cahoy[2,5]**

[1]Department of Astronomy/Steward Observatory, University of Arizona, Tucson, AZ, United States, [2]Department of Aeronautics and Astronautics, Massachusetts Institute of Technology, Cambridge, MA, United States, [3]Department of Physics, California Institute of Technology, Pasadena, CA, United States, [4]Aurora Flight Sciences, Cambridge, MA, United States, [5]Department of Earth, Atmospheric and Planetary Sciences, Cambridge, MA, United States

OPEN ACCESS

**Edited by:**
Simon Pete Worden,
Other, United States

**Reviewed by:**
Erick T Young,
Universities Space Research Association (USRA), United States
P. S. Athiray,
NASA Postdoctoral Program, United States

***Correspondence:**
Ewan S. Douglas
douglase@arizona.edu
Kerri L. Cahoy
kcahoy@mit.edu

**Specialty section:**
This article was submitted to Astronomical Instrumentation, a section of the journal Frontiers in Astronomy and Space Sciences

**Received:** 05 March 2021
**Accepted:** 12 July 2021
**Published:** 26 August 2021

**Citation:**
Douglas ES, Allan G, Morgan R, Holden BG, Gubner J, Haughwout C, do Vale Pereira P, Xin Y, Merk J and Cahoy KL (2021) Small Mirrors for Small Satellites: Design of the Deformable Mirror Demonstration Mission CubeSat (DeMi) Payload. Front. Astron. Space Sci. 8:676281. doi: 10.3389/fspas.2021.676281

The Deformable Mirror Demonstration Mission (DeMi) is a technology demonstration CubeSat to test a 140 actuator micro-electromechanical system (MEMS) deformable mirror in low-Earth orbit. Such mirrors can provide precise wavefront control with low size, weight, and power per actuator. Hence, they have the potential of improving contrast in coronagraphs on future space telescopes. In the DeMi payload, a Shack Hartmann lenslet array based wavefront sensor monitors the deformable mirror, illuminated by either an internal 636 nm laser diode or external starlight. This work describes the instrument design drivers and CubeSat implementation, and briefly illustrates operation on orbit by comparing ground-based measurements of a displaced actuator to an on-orbit measurement using the internal laser source. The 6U CubeSat was launched on February 25, 2020 and deployed from the International Space Station on July 13, 2020.

**Keywords: astrophysics, MEMS, wavefront sensing, CubeSats, deformable mirror, wavefront control, space telescopes**

## 1 INTRODUCTION

This work provides an overview of the design considerations and engineering of the Deformable Mirror Demonstration Mission optical payload. Details of the implementation are provided to establish technology readiness level (TRL) and provide a foundation for understanding future application of active wavefront control on satellites.

Deformable mirrors which actively change shape at sub-wavelength precision have a wide array of applications in space, such as future missions to image Earth-like exoplanets (Levine et al., 2009; Stapelfeldt et al., 2014; Pueyo et al., 2019; Ruane et al., 2019; Gaudi et al., 2020; Kasdin et al., 2020), correction of scattered light imaging of dim debris disks (Chakrabarti et al., 2015; Cook et al., 2015; Sirbu et al., 2015; Douglas et al., 2018; Maier et al., 2020), reconfigurable telescopes (Underwood et al., 2015), and error correction for deployable or inflatable apertures (Dolkens et al., 2019; Lesser et al., 2019). Micro-electromechanical systems (MEMS) Deformable Mirror (DM)s are included in designs for many future exoplanet imaging missions due to relatively high actuator counts which allow correction of high-order spatial errors, and low Size, Weight, and Power (SWaP) (Pueyo et al., 2019). For a detailed review of MEMS operation and testing in space and space-like environments see Morgan et al. (2019).

While much of the interest in DM technology in space has been for large-scale missions with apertures of several meters or larger, there is a large continuum of nanosatellite applications for the technology. These include correcting thermal and deployment errors on future small space telescopes (e.g. Maier et al. (2020)), wavefront control for optical space interferometry, and biological and *in-vivo* microscopy (Bifano, 2011; Wahl et al., 2015; Marx, 2017) in space. Closely related to the continuous phase-sheet mirrors described here are segmented deformable mirrors, which allow other applications such as image slicing and data transmission (Chan and Ford, 2006).

The DeMi mission goal is to demonstrate MEMS mirror operation in space for an extended period of time. The DeMi payload has evolved over several years in order to improve the design fidelity, redundancy, and versatility of the instrument (Cahoy et al., 2013a; Marinan and Cahoy, 2014; Marinan, 2016; Marinan et al., 2016; Douglas et al., 2017; Allan et al., 2018; Morgan, 2019). The final optical and electronics design was an iterative process which was not complete until final integration and testing. The DeMi payload was assembled for flight in the Summer-Fall of 2019. The final payload design contains a 35-mm primary mirror, an internal calibration laser light source, a 140-actuator Multi MEMS DM from Boston Micromachines Corporation (BMC), a Shack Hartmann wavefront sensor, and an image plane wavefront sensor. The DeMi mission underwent environmental testing in Fall 2019 and was launched in February 15th, 2020. In-space operations began in July of 2020 after deployment from the International Space Station (ISS). Detailed analysis of on-orbit performance and trends are ongoing and will be presented in future work.

This manuscript summarizes the design drivers [**Section 2**], the engineering constraints [**Section 3**], the as-flown design [**Section 4**], the first-light results on-orbit [**Section 5**], and future directions [**Section 6**].

## 2 DESIGN DRIVERS

This section describes the key mission requirements that drove the design of the DeMi payload. As a technology demonstration CubeSat, the DeMi payload's primary goal is to establish the survivability of MEMS DMs for launch, extended operation in a low-earth orbit (LEO) orbit, particularly the vacuum, thermal, and radiation environment, and to raise the technology readiness level (TRL) of MEMS DM hardware from TRL six to at least seven (Cahoy et al., 2013b; Morgan et al., 2019). To meet this goal, the DeMi payload design was required to precisely monitor the response of the MEMS to the orbital environment, which necessitated the measurement of mirror operation prior to launch and over the approximately year-long mission.

### 2.1 Measuring Actuator Response

In order to characterize the behavior of the DM prior to and in flight, the payload was required to be capable of measuring the response of actuators at or below the level of typical MEMS DM manufacturing error, 10–20 nm root mean squared (RMS) (Evans et al., 2006; Morzinski et al., 2012). This requirement tests absolute actuation in open-loop operation.

### 2.2 Measure and Correct Wavefront Phase Aberrations in Space

The DeMi optical payload is designed to demonstrate closed-loop wavefront control in space, correcting thermally driven aberrations (e.g. focus and astigmatism), as well as spacecraft pointing errors. The DeMi payload is designed to correct both static and dynamic wavefront errors to less than 100 nm RMS. Closed-loop, in-space wavefront control with a MEMS DM is currently at a TRL of 5–6 (Cahoy et al., 2013a; Sirbu et al., 2015; Morgan et al., 2019; Prada et al., 2019), and DeMi is designed to raise this TRL using on-orbit performance data. This requirement tests closed-loop Adaptive Optics (AO) operation.

## 3 ENGINEERING CONSTRAINTS

In addition to the classic CubeSat constraints on SWaP (Heidt et al., 2000), implementing an adaptive optics system on a CubeSat introduces several additional constraints that define the DeMi payload design. The DeMi adaptive optics layout was informed by many ground-based instruments, particularly those built around similar 12 × 12 DMs and lenslet-based wavefront sensors such as the Lick Observatory Villages (Morzinski et al., 2012) and the Robo-AO instruments (Baranec et al., 2012, 2013). A 6U CubeSat with 4U available for the payload was found to be the minimum size that could accommodate the factors described below.

### 3.1 Actuator Stroke

While many high-contrast mission designs include a Fast Steering Mirror (FSM) upstream of the DM to provide precision pointing correction (e.g. Roberts et al. (2013); Chakrabarti et al. (2015); Demers et al. (2015)), the volume requirements of a CubeSat platform suggest an all-in-one design where the DM provides both pointing and high-order correction. Continuous phase-sheet MEMS DM stroke depends on the displacement of adjacent actuators (Bifano et al., 1997); thus, a conservative margin was applied to determine the stroke required to correct for misalignments as well as spacecraft pointing errors using a Blue Canyon XACT attitude determination and control system (ADCS) which were assumed to be $\lesssim 10''$ RMS (Mason et al., 2016).

### 3.2 Pupil Size

In order to illuminate the deformable mirror and place it in a conjugate plane to the input pupil, an image of the input optical pupil must be formed on the DM. The size of this pupil in the system sets the magnification of the astronomical telescope. MEMS DM actuators are ~300–500 microns across and the actuator stroke depends on the size of the actuators (smaller actuators having shorter stroke due to the increased actuation force required). Smaller actuators sizes also require a higher telescope magnification, increasing optomechanical alignment sensitivity. The telescope entrance aperture size and magnification was set to underfill the mirror by 10% to allow for payload shifts. The magnification and entrance aperture

diameter were also constrained by alignment tolerances, limited by the ability of commercially available M2.5 x 0.20 adjustment screws to set the system to within $<\lambda/4$ wavefront error (as determined by Zemax ray-tracing), and ensure the stroke was not limited by edge actuators.

## 3.3 Pixel Size

The pixel size of the cameras determined the accuracy of centroiding for the Shack-Hartmann Wavefront Sensor (SHWFS) (for basics of operation, see Tyson and Frazier (2004)) and the sensitivity of the image plane wavefront sensor. The DeMi concept of operations does not include on-orbit flat fielding, and radiation is expected to change the pixel responsivity; thus, photo response non-uniformity (PRNU) sets a lower limit on the noiseless SHWFS accuracy. To verify that the SHWFS system met wavefront sensitivity requirements, PRNU variation up to and exceeding the 5 kRad doses tested by Becker et al. (2008) were simulated with the realistic lenslet point spread functions (PSFs) (Generated in POPPY Perrin et al. (2016); Morgan (2020).). The center of mass of these PSFs were calculated as a function of increasing PRNU to show <0.1 pixel centroiding would be achieved even after irradiation and without flat-fielding (Douglas et al., 2017).

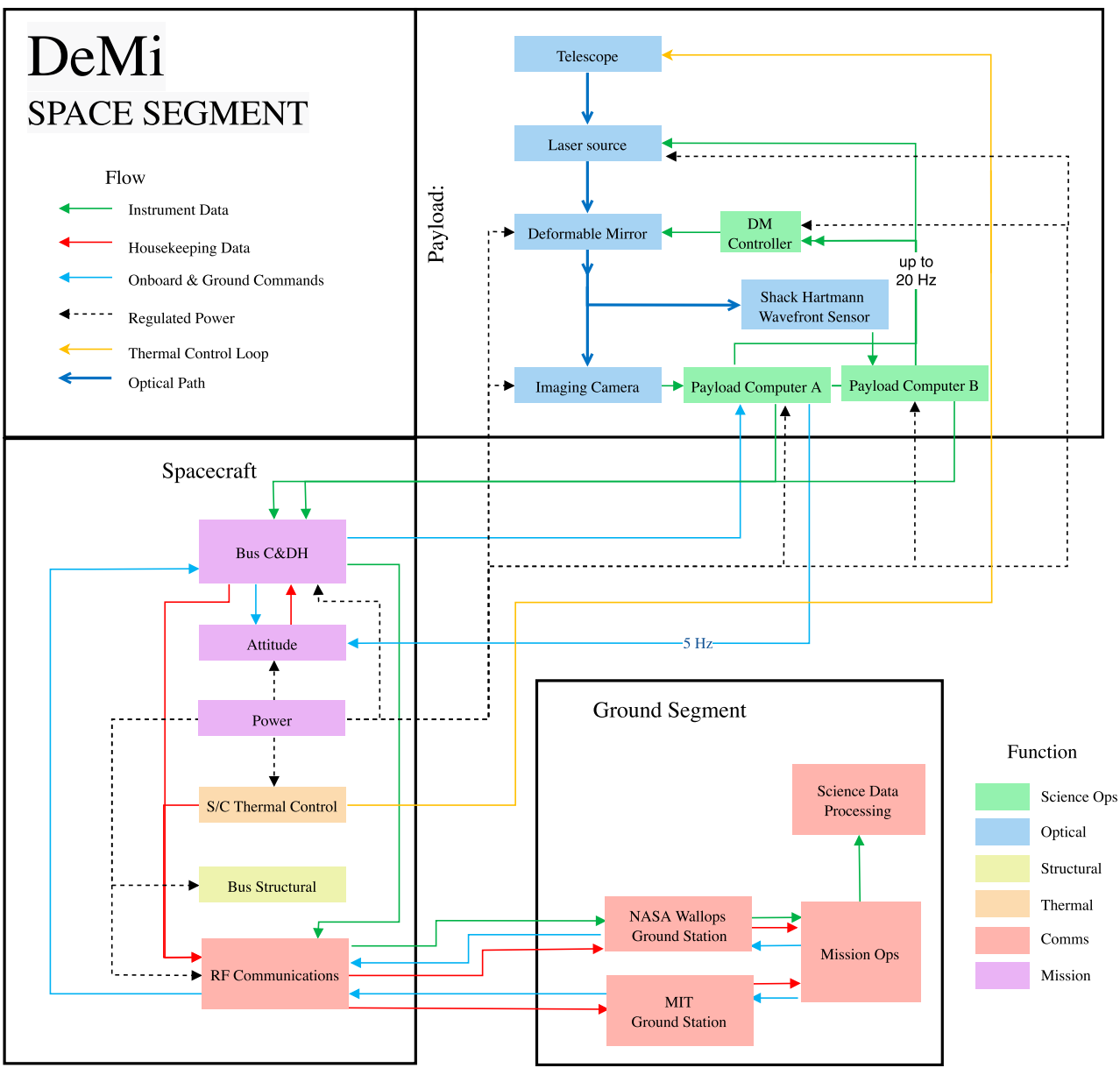


**FIGURE 1 |** DeMi mission level block diagram. The optical path (**Figure 2**) is shown as thick blue arrows, all other paths are communications or power). Multiple electrical pathways, sensors, and payload computers to control the DM were implemented to maximize redundancy and improve the likelihood of mission success.

**TABLE 1 |** Table of Optical Components. D is the clear aperture of each optic and fl is the effective focal length. RMSE errors are specified in surface units. DM and Field mirror surface errors are measured, others are manufacturer spec at $\lambda$ = 633 nm. NA specs are is not applicable to the part.

| ID | Component | D/fl [mm] | RMSE Surface | Substrate + Coating | Model |
|---|---|---|---|---|---|
| EA | Entrance aperture and baffle | 30/Na | NA | Ultem 9,085 (Black) + NA | Custom: Xometry 3D print |
| M1 | Primary OAP | 35/100 | $\lambda$/8 | Al + $SiO_2$ | Custom: Thorlabs |
| FM | Field mirror | NA/NA | 10 nm | Al + $SiO_2$ | Custom: Surface finishes, Addison, Illinios |
| M2 | Collimating OAP | 8.5/15 | $\lambda$/4 | Al + $SiO_2$ | Custom: Thorlabs |
| DM | Deformable mirror | 4.95/NA | 16.8 nm | Silicon + Gold | BMC 5.5 $\mu$m Multi-DM |
| BS | Beamsplitter | 12.5/NA | $\lambda$/10 | Fused silica | Thorlabs BSN04 |
| IL | Imaging lens | 12.5/25 | | N-LAK8 +AR/N-SF57 | Edmund optics 49–660 |
| R1 | 1st relay OAP | 12.7/50 | $\lambda$/8 | Al + $SiO_2$ | Custom: Thorlabs |
| R2 | 2nd relay OAP | 12.7/50 | $\lambda$/8 | Al + $SiO_2$ | Custom: Thorlabs |
| SHWFS | Lenslet array | 0.15/4.1 | | Fused silica and Chrome Mask | Thorlabs MLA150-5C |
| SMF | Single mode fiber | NA | NA | Fused silica | Thorlabs SM600 |
| LD | Laser diode | NA | NA | NA | Thorlabs LPS-635-FC |
| Sensors | CMOS sensors | NA/4.2 × 5.7 | NA | NA | PixeLink CMOS PL-D775MU-BL |

# 4 PAYLOAD IMPLEMENTATION

This section describes the implementation of the DeMi payload, highlighting the additional drivers that influenced design decisions. A diagram of the DeMi payload and mission architecture is shown in **Figure 1**. Light enters through the primary aperture for external observations or through an single mode optical fiber, injected at the field mirror for internal calibration measurements. Light from either source reflects off of the MEMS DM and is then split between the image plane wavefront sensor, which records PSFs, and the Shack Hartmann wavefront sensor, which measures centroid displacements that can be reconstructed to provide a map of wavefront error. **Table 1** summarizes the system optical prescription and related components, details of which are below and **Table 2** summarizes key instrument parameters.

## 4.1 Redundancy

In-order to ensure mission success, emphasis was placed on redundancy at every level of the payload design, from optical paths to electronic subsystems: DeMi has two radio transmitters, two computers, two cameras, and two light sources (stars and an internal laser). The system was also required to allow reprogramming of the payload software while on orbit to test new control algorithms and fix any bugs that were not discovered on the ground.

## 4.2 Deformable Mirror

In selecting a DM for the DeMi mission, a desire to maximize the number of actuators and improve the statistical power of the experiment was balanced against limitations in pupil size and controller electronics SWaP. A Boston Micromachines Multi-DM with 140 actuators and rated actuator stroke of 5.5 $\mu$m was selected for the mission. Actuator stroke is rated for 255 V and for four actuators together in piston. The mirror stroke, $S$ was selected to provide sufficient tip-tilt wavefront control to correct for spacecraft pointing errors of <10″ after derating the stroke by the 40 degree-from-normal angle of incidence on the DM and the controller maximum voltage of 150 V (Morgan, 2019). Thus, the maximum tilt correction was calculated as $(2\cos(40\ \text{deg})S/D$, where the factor of two is included because stroke is surface motion, not wavefront tilt. This predicted correction up to 11″, which provided little margin on 10″ pointing error. Thus, to further mitigate spacecraft pointing errors, offloading of pointing errors at 1 Hz or greater to the XACT was a requirement levied on the spacecraft by the payload (**Figure 1**). This is consistent with the slow, thermally driven behavior of large pointing excursions which as been observed on the XACT (Pong, 2018; Knapp et al., 2020).

## 4.3 Optical Train

The optical path is shown in **Figure 2**. A largely aluminum optical train was designed in order to minimize chromatic aberrations and coefficient of thermal expansion (CTE) mismatches. Reflective optics were all polished aluminum with $SiO_2$ protective coatings, and directly bolted to the 7075-alloy aluminum structure. Custom diamond turned off-axis parabola (OAP) mirrors, with focal lengths and bolt patterns matching commercial off-the-shelf (COTS) parts, allowed for flexibility and the rapid construction of a fully functional optical test bed and optically functional 3D printed models as described in Gubner (2018). As an approximation for launch loads, the optical train was designed to survive 100 g static loading. The optomechanical and thermal design of the payload are detailed in

**TABLE 2 |** DeMi payload parameters.

| Parameter | Value |
|---|---|
| Primary aperture | 30 mm |
| Pixel size | 2.2 $\mu$m |
| Imager resolution | 6″ |
| Half-angle imager FOV | 0.7deg |
| Imager plate scale | 2.7″/pix |
| Lenslet sampling | 150 $\mu$m |
| DM actuator size | 450 $\mu$m |
| DM | 12 × 12 |
| Lenslet/Actuator sampling | 3 |
| DM controller resolution | 14 bit |
| DM controller voltage range | 0–150 V |
| Measured single actuator DM stroke | 1 $\mu$m |
| Measured four actuator DM stroke | 2.8 $\mu$m |

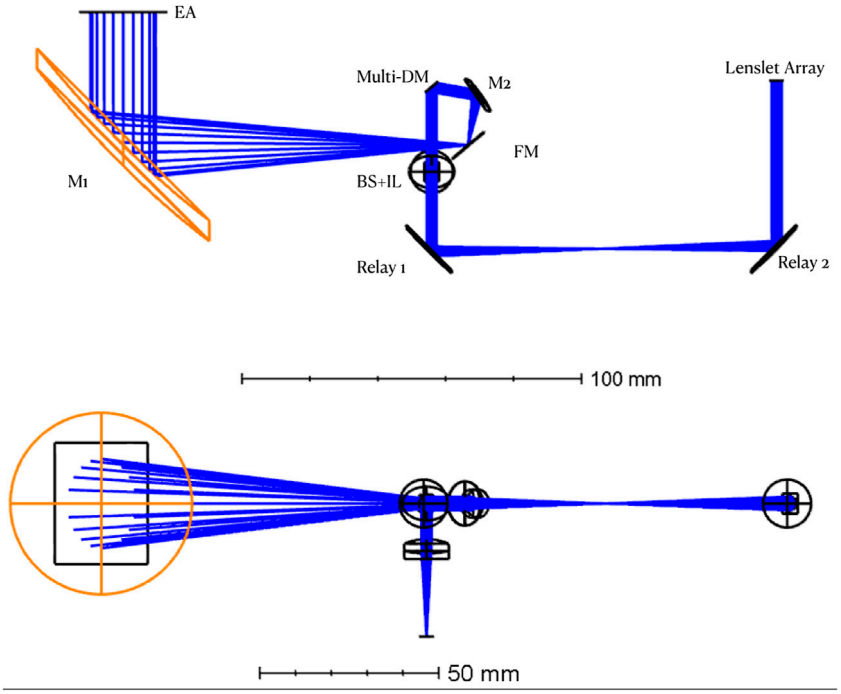


**FIGURE 2 |** Top and side ray traces of the DeMi optical layout. EA (entrance aperture) is defined at the baffle output. OAPs M1 and M2 relay an image of that pupil to the surface of the Multi DM, the output collimated beam from which is split by a beamsplitter (BS) between an imaging lens (IL) and second pair of OAPs which relay an image of the DM surface to the lenset array which acts as a SHWFS. See **Table 1** for component level specs and **Table 2** for system parameters.

Allan et al. (2018); do Vale Pereira, (2020). **Figure 4** shows the engineering model, which was built to flight-specifications including surface finishes and optical components, and was fully integrated with a functional deformable mirror and other sensors. The engineering model was used for mechanical and fit-testing, software development, and as a source of flight-spare components. The flight unit, **Figure 4**, was slightly refined to raise the first structural mode, as detailed in do Vale Pereira, (2020).

### 4.3.1 Baffle

In order to maximize stray-light rejection in the available volume, a simple baffle (Arnoux, 1996) was designed with a 25° exclusion angle and a second vane added to provide a 45° secondary exclusion of bright off-axis sources.

### 4.3.2 Field Mirror

The field mirror is a critical piece of the DeMi optical design that allows for testing of DM operations on both stars and the internal laser diode without moving parts or complex dichroic beam paths. This design provides redundancy since laser failure does not prevent stellar observations, and failure of spacecraft ADCS does not prevent laser operation and mirror metrology. The field mirror is composed of two pieces of super-polished aluminum with an embedded single-mode optical fiber. Field mirror surface errors manifest as beamwalk on the DM and vignetting. The DeMi payload requires that no more than a 5% shift of the beam relative to the DM active area, or no more than one approximately half an actuator of beamwalk, should occur. This set a mirror surface finish requirement of ~6 nm RMS on $\lambda/D$ spatial scales (~2 $\mu$m) at the field mirror. The delivered mirror's overall surface is 10 nm root mean squared error (RMSE), which is dominated by infrequent aluminum grains which produce ~200 nm peaks and pits. The field mirror was designed to place the fiber tip 0.2° from the optimal ray path through the payload, placing it within the field of view of the telescope, inside the diffraction limited field of view (which was required to be 0.2 deg half-width) and the dynamic range of the SHWFS calculated from the lenslet focal length and aperture (see Chanan (2000); Tyson and Frazier (2004)).

### 4.3.3 Imaging Lens

The only refractive free-space optical components are the lenslet array and the imaging lens (IL). A COTS achromatic lens was chosen to provide a wide field of view (~1 deg) to better accommodate changes in co-alignment between the spacecraft ADCS and the payload. The imaging path provides redundant wavefront sensing and control, as the DeMi design includes both a Shack Hartmann wavefront sensor that records centroid measurements in a pupil plane and an image plane wavefront sensor that records PSFs (Allan, 2018).

## 4.4 Sensors and Readout Electronics

Pixel size was a key design driver to enable precision wavefront sensing in the CubeSat volume. A PixeLink CMOS PL-D775MU-BL MONO 1/2.5 in, with a monochromatic ON Semiconductor MT9P031 CMOS sensor, was selected for both the Shack

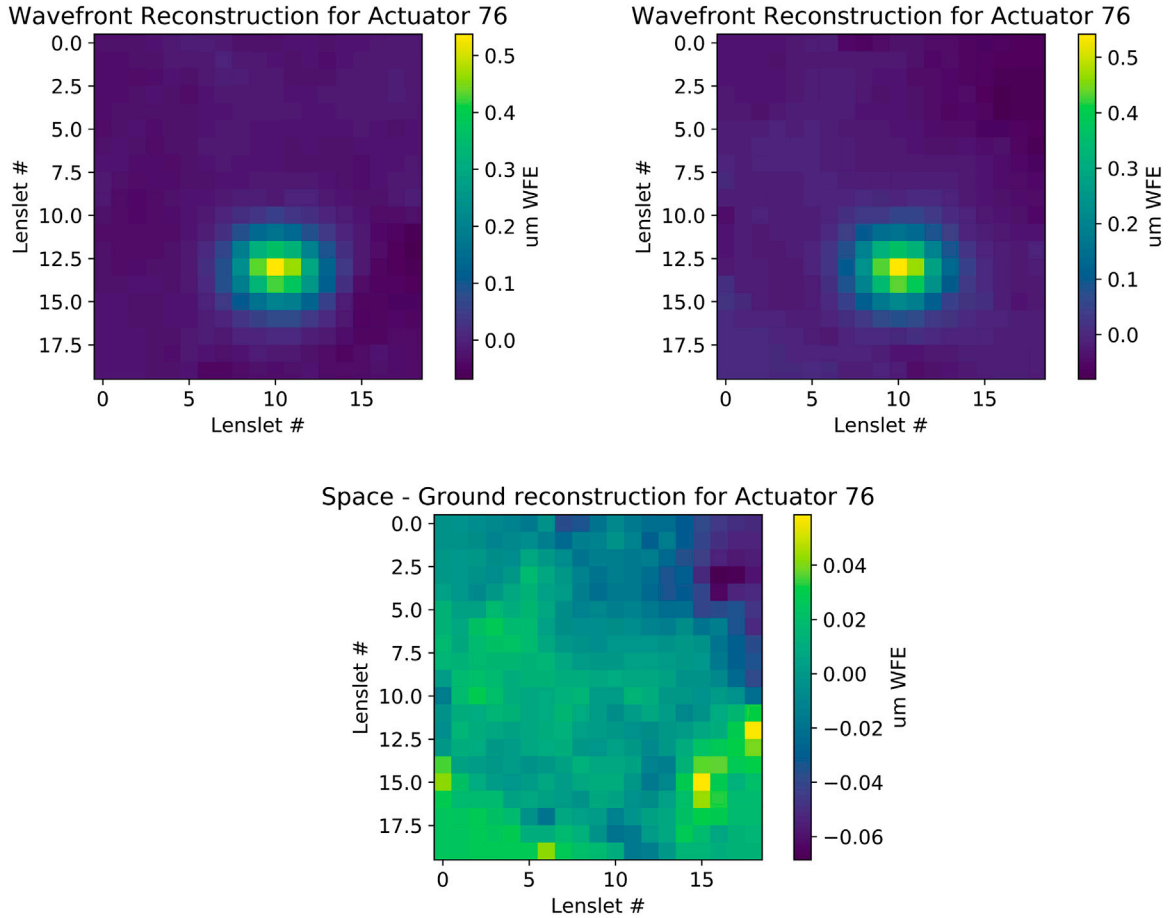


**FIGURE 3 | Top left:** reconstructed SHWFS measurement of single actuator poke on the ground prior to launch. **Top right:** reconstruction of the same actuator poked in space. Both tests were recorded using all flight hardware and the internal laser diode source. See Morgan et al. (2021) for details of the instrument calibration on the ground and in orbit. **Bottom:** the residual difference in reconstructed wavefront between the space and ground measurements.

Hartmann wavefront sensor and the image plane wavefront sensor. The MT9P031 has been radiation tested (Becker et al., 2008) and has extensive flight heritage as part of the Sinclair Interplanetary Star Tracker (Enright et al., 2011; Sinclair et al., 2015).

The MT9P031 has 2.2 micron pixels and this pixel size set the imaging lens (IL) focal length, since two pixels per $\lambda/D$ resolution spot were desired to allow coarse image plane wavefront sensing (Codona, 2013; Allan, 2018). Each sensor is read out by a separate camera board connected to each of the two cross-strapped Raspberry Pi 3 modules that serve as payload computers. Each Raspberry Pi 3 contains two identical SD cards that can be used interchangeably in the event of radiation damage impacting memory or flight software.

The imaging system needed for PSF measurement provides a model of a typical in-space instrument whose operation would benefit from AO technology. Closed-loop wavefront control on a broadband stellar source fully demonstrates the feasibility of AO with MEMS DMs in space. The requirement also highlights potential usefulness of actively corrected telescopes like DeMi as tools for science, as accurate pointing correction on nanosatellites enables photometric observation of transiting exoplanets, as in (Knapp et al., 2020).

# 5 MISSION STATUS

## 5.1 Integration and Test

The optical system was aligned end-to-end using a Zygo Verifire interferometer. The optical payload was aligned in segments, and end-to-end system tests with the calibration laser inserted in the field mirror were conducted periodically throughout alignment to ensure the optical fiber laser signal was kept inside the imager FOV and within the SHWFS capture range. The end-to-end system was aligned to $<0.25\lambda$ wavefront error with the DM in the unpowered position (all actuators commanded to 0 V). As described in do Vale Pereira, (2020), an engineering model of the payload was vibration tested. As seen in **Figure 4**, the

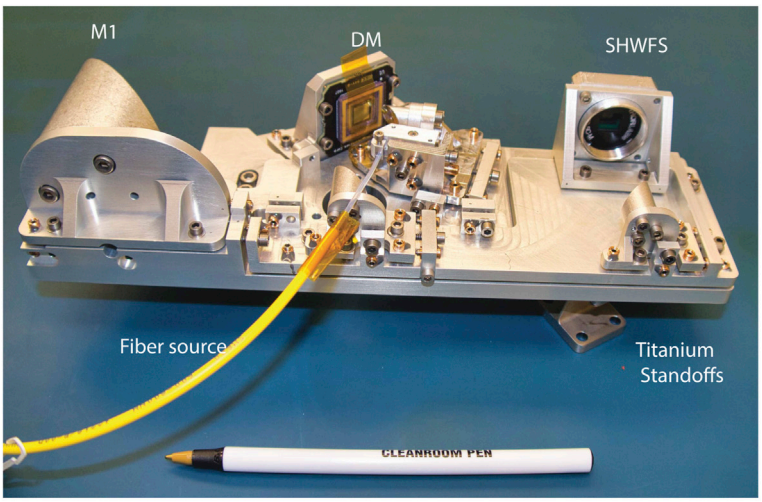


Fully Functional Engineering Model

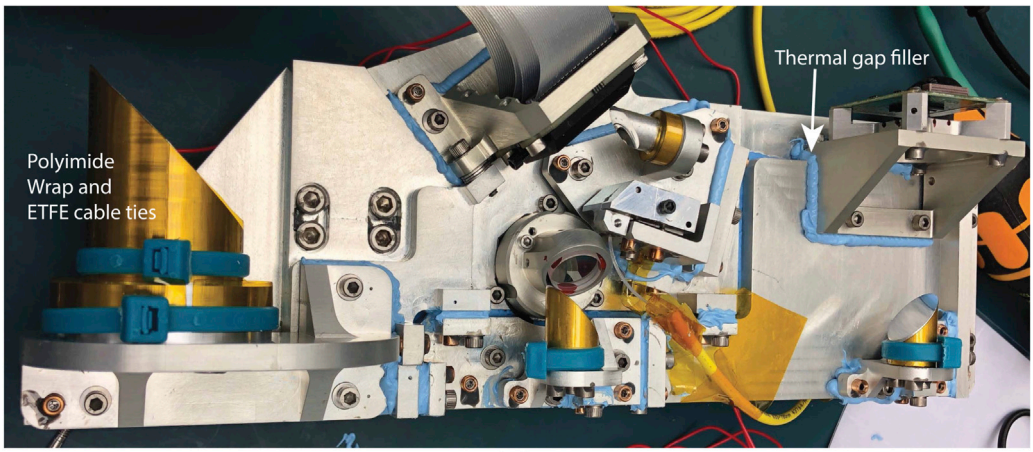


Flight Unit

**FIGURE 4 |** Two fully function payload units were constructed to enable an iterative engineering approach. **Top:** A payload engineering model was built to flight specifications to demonstrate optical performance, test wavefront sensing and control software, and to provide spare parts for flight. **Bottom:** assembled flight model. (The yellow Hytrel fiber jacket protected the test fiber and was not flown).

aluminum optics were wrapped in polyimide tape to increase emissivity and thermal gap filler was added to minimize temperature gradients across the payload. he M1 mirror diameter reduced and the flight structure was also modified to increase stiffness, as described in do Vale Pereira, (2020). The aligned flight model of the payload was integrated into the spacecraft bus and was subjected to standard CubeSat thermal and mechanical cycling (described in do Vale Pereira, (2020)) prior to delivery to the launch services provider in December 2019.

## 5.2 Launch and Deployment

DeMi was launched to the ISS on February 15, 2020 aboard the Cygnus NG-13 flight of Northrop Grumman from NASA's Wallops Flight Facility. DeMi was deployed on July 13, 2020 as shown in **Figure 5**. The overall flow of signals through DeMi is shown in **Figure 1**. The upper right box is the payload subsystem described here, which passes data to and receives data from the spacecraft bus (lower left), which provides communication to ground segment at MIT and NASA Wallops. Initial checkout data from August 4, 2020 shows the DM illuminated by the internal laser diode and measured with the Shack Hartmann wavefront sensor. A reconstruction of this wavefront measurement compared to similar data from ground testing is shown in **Figure 3**. From October 8, 2020 UHF ground station mechanical issues at NASA Wallops Flight Facility prevented science data downlinks; however, a low-data-rate ground station located at the MIT campus was been used to monitor spacecraft health and downlink a small set of payload data. Following to Wallops return to service on March 22, 2021, DeMi

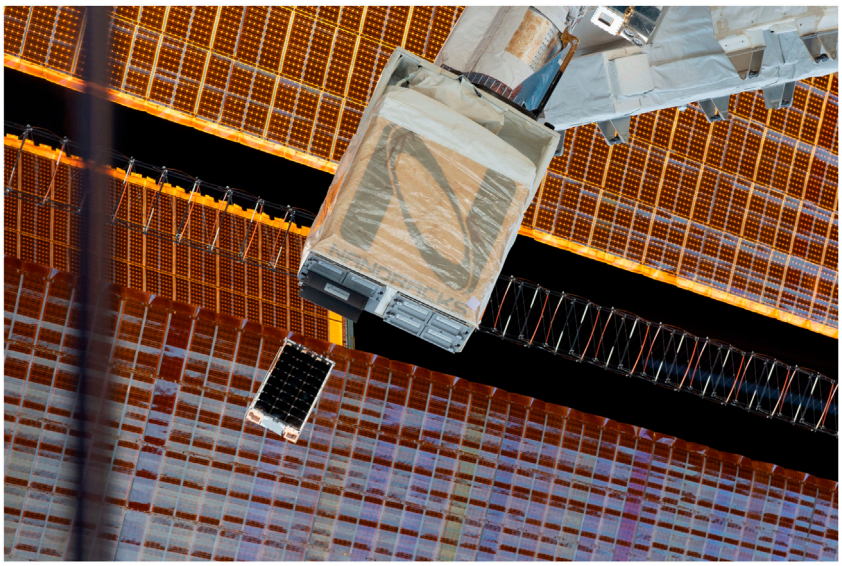

**FIGURE 5 |** DeMi CubeSat being deployed from the International Space Station. Image "iss063e044976" from the ISS Cupola, courtesy NASA.

commissioning has resumed and will be the subject of future publications.

Planned deformable mirror commisioning tests include: application and testing of pre-recorded Zernikes, image-plane wavefront sensing, and repeating the actuator poke test illustrated in **Figure 3** for all actuators to monitor stability and function over time. **Figure 3** shows a single actuator set to 60 V referenced to flat map. 60 V approximately corresponds to one wave of wavefront error at the test laser wavelength. The left panel shows a ground measurement and the right panel shows the flight measurement. The difference between the space and ground measurements of the same actuator is shown in the center bottom panel and has an RMS of 21 nm. This reported error includes all lenslets across the SHWFS, some of which are poorly illuminated, and contribute to excess error. For details on the accuracy and precision with which all actuators are calibrated and measured see Morgan et al. (2021).

## 6 DISCUSSION

Since DeMi was designed there has been significant progress in MEMS-based wavefront control, which bodes well for future missions with higher actuator counts. Prada et al. (2019) demonstrated stable 5e-9 contrast in vacuum with a 32 × 32 MEMS mirror combined with a Vector Vortex Coronagraph (VVC) (Mawet et al., 2010). Bendek et al. (2020) has developed and tested a CubeSat-scale MEMS deformable mirror controller that controls 32 × 32 actuators and survived flight on the PICTURE-C ballon.

The DeMi mission is currently demonstrating a MEMS DM in space and assessing its response to the orbital environment. It will also demonstrate closed-loop wavefront control on a CubeSat. The results from this mission will be useful for future spacecraft designers working on a range of applications. Particularly, DeMi is designed to retire several risks in space high-contrast imaging, raising the TRL of MEMS deformable mirrors. The DeMi mission is also demonstrating a COTS-based DM controller architecture that is scalable to future applications requiring higher actuator count MEMS DMs (Haughwout, 2018).

## DATA AVAILABILITY STATEMENT

The raw data supporting the conclusion of this article will be made available by the authors, without undue reservation.

## AUTHOR CONTRIBUTIONS

ED, GA, RM, JG, PP, and YX contributed to payload design, simulation, integration, test, and manuscript preparation. BH, and CH and contributed to payload design, simulation, integration, and test. KC is the DeMi payload PI and JM is the mission PI, both contributed to payload and mission conception and design.

## FUNDING

This material is based upon work supported by the Defense Advanced Research Projects Agency (DARPA) Program Office under Contract No. W31P4Q-16-C-0089. The DeMi mission is managed by Aurora Flight Sciences (Aurora Subcontract: AMA-19-0015). The DeMi spacecraft bus was built under contract by Blue Canyon Technologies. RM is a NASA Space

Technology Research Fellow under grant 80NSSC18K1182. YX is a NSF Graduate Research Fellow under grant 1122374. Portions of ED contribution to this work were supported by the Arizona Board of Regents Technology Research Initiative Fund (TRIF).

## ACKNOWLEDGMENTS

The DeMi program has trained approximately one dozen graduate students in space astronomy, wavefront sensing, CubeSat design, and mission operations. These efforts have led to numerous student theses at the PhD (Marinan, 2016), masters (Allan, 2018; Haughwout, 2018; Morgan, 2020), and bachelor-degree levels (Gubner, 2018). The authors thank the Boston University Scientific Instruments Facility for their contributions to the hardware as well as Felipe Depine (Robots5), Kerry Gonzales and Bohan Li (UArizona), as well as thanks to Mark Egan, Gabor Furesz, and Becky Masterson (MIT) for advice and engineering inputs. Nanoracks LLC was the launch provider contracted for the DeMi spacecraft and provided useful equipment and instruction for spacecraft vibration testing. The MIT Kavli Institute generously provided access to an interferometer and clean room space for DeMi alignment and spacecraft testing.

## REFERENCES

Allan, G., Douglas, E. S., Barnes, D., Egan, M., Furesz, G., Grunwald, W., et al. (2018). The Deformable Mirror Demonstration mission (DeMi) CubeSat: Optomechanical Design Validation and Laboratory Calibration. *Proc. SPIE* 10698, 1069857, 2018. International Society for Optics and Photonics.

Allan, G. W. (2018). *Simulation and Testing of Wavefront Reconstruction Algorithms for the Deformable Mirror (DeMi) Cubesat*. Cambridge, MA: Masters Thesis, Massachusetts Institute of Technology.

Arnoux, J.-J. P. (1996). Star Sensor Baffle Optimization: Some Helpful Practical Design Rules. *Proc. SPIE*, 333–338. doi:10.1117/12.258324

Baranec, C., Riddle, R., Law, N. M., Ramaprakash, A. N., Tendulkar, S. P., Bui, K., et al. (2013). Bringing the Visible Universe into Focus with Robo-AO. *J. Vis. Exp.* 72. 50021. doi:10.3791/50021HTML

Baranec, C., Riddle, R., Ramaprakash, A. N., Law, N., Tendulkar, S., Kulkarni, S., et al. (2012). Robo-AO: An Autonomous Laser Adaptive Optics and Science System. *Imaging and Applied Optics, OSA Technical Digest (CD) (Optical Society of America, Adaptive Optics: Methods, Analysis and Applications 2011 Toronto Canada 2011),* Paper AWA2.

Becker, H. N., Dolphin, M. D., Thorbourn, D. O., Alexander, J. W., and Salomon, P. M. (2008). *Commercial Sensory Survey Radiation Testing Progress Report*. Pasadena, CA: Jet Propulsion Laboratory, National Aeronautics and Space Administration.

Bendek, E., Ruane, G., Prada, C. M., Mendillo, C. B., Riggs, A. J. E., and Serabyn, E. (2020). Microelectromechanical Deformable Mirror Development for High-Contrast Imaging, Part 1: Miniaturized, Flight-Capable Control Electronics. *JATIS* 6, 20. doi:10.1117/1.jatis.6.4.045002

Bifano, T. G., Mali, R. K., Dorton, J. K., Perreault, J., Vandelli, N., Horenstein, M. N., et al. (1997). Continuous-membrane Surface-Micromachined Silicon Deformable Mirror. *Opt. Eng.* 36, 1354–1360. doi:10.1117/1.601598

Bifano, T. (2011). MEMS Deformable Mirrors. *Nat. Photon* 5, 21–23. doi:10.1038/nphoton.2010.297

Cahoy, K. L., Marinan, A. D., Novak, B., Kerr, C., Nguyen, T., Webber, M., et al. (2013a). MEMS Deformable Mirror CubeSat Testbed. *Proc. SPIE* 8864, 88640U–88640U–88717U. doi:10.1117/12.2024684

Cahoy, K. L., Marinan, A. D., Novak, B., Kerr, C., and Webber, M. (2013b). Wavefront Control in Space with MEMS Deformable Mirrors. *Proc. SPIE* 8617, 861708–861708–16. doi:10.1117/12.2005685

Chakrabarti, S., Mendillo, C., and Cook, T. A. (2015). *Planet Imaging Coronagraphic Technology Using a Reconfigurable Experimental Base (PlCTURE-B): The Second in the Series of Suborbital Exoplanet Experiments*. Journal of Astronomical Instrumentation Submitted.

Chan, T. K., and Ford, J. E. (2006). Retroreflecting Optical Modulator Using an MEMS Deformable Micromirror Array. *J. Lightwave Technol.* 24, 516–525. doi:10.1109/jlt.2005.859853

Chanan, G. (2000). *Principles of Wavefront Sensing and Reconstruction*. Santa Cruz, CA: Center for Adaptive Optics (CfAO) Proceedings: Summer School on Adaptive Optics.

Codona, J. L. (2013). Differential Optical Transfer Function Wavefront Sensing. *Opt. Eng.* 52, 097105. doi:10.1117/1.OE.52.9.097105

Cook, T., Cahoy, K., Chakrabarti, S., Douglas, E., Finn, S. C., Kuchner, M., et al. (2015). Planetary Imaging Concept Testbed Using a Recoverable Experiment-Coronagraph (PICTURE C). *J. Astron. Telesc. Instrum. Syst.* 1, 044001. doi:10.1117/1.JATIS.1.4.044001

Demers, R. T., Dekens, F., Calvet, R., Chang, Z., Effinger, R., Ek, E., et al. (2015). Requirements and Design Reference mission for the WFIRST/AFTA Coronagraph Instrument. *In Tech. Instrumentation Detect. Exoplanets VII* 9605, 960502. 2015. International Society for Optics and Photonics. doi:10.1117/12.2191792

do Vale Pereira, P., Holden, B., Morgan, R., Gubner, J., Murphy, T. J., Haughwout, C., et al. (2020). Thermomechanical Design and Testing of the Deformable Mirror Demonstration Mission (DeMi) CubeSat. In 34th Annual Small Satellite Conference.

Dolkens, D., van Marrewijk, G., and Kuiper, H. (2019). "Active Correction System of a Deployable Telescope for Earth Observation," in International Conference on Space Optics — ICSO 2018, 11180. Chania, Greece: International Society for Optics and Photonics, 111800A. doi:10.1117/12.2535929

Douglas, E. S., Cahoy, K. L., Merck, J., Barnes, D., Allan, G., Skouloudis, N., et al. (2017). Design of the Deformable Mirror Demonstration CubeSat (DeMi). *Proc. SPIE* 10400, 1040013. doi:10.1117/12.2274430

Douglas, E. S., Mendillo, C. B., Cook, T. A., Cahoy, K. L., and Chakrabarti, S. (2018). Wavefront Sensing in Space: Flight Demonstration II of the PICTURE Sounding Rocket Payload. *J. Astron. Telesc. Instrum. Syst.* 4, 1. doi:10.1117/1.JATIS.4.1.019003

Enright, J., Sinclair, Doug., and Fernando, Christy. (2011). *COTS Detectors for Nanosatellite Star Trackers: A Case Study*. Logan, UT: Utah State University: DigitalCommons@USU.

Evans, J. W., Macintosh, B., Poyneer, L., Morzinski, K., Severson, S., Dillon, D., et al. (2006). Demonstrating Sub-nm Closed Loop MEMS Flattening. *Opt. Express* 14, 5558–5570. doi:10.1364/oe.14.005558

Gaudi, B. S., Seager, S., Mennesson, B., Kiessling, A., Warfield, K., Cahoy, K., et al. (2020). *The Habitable Exoplanet Observatory (HabEx) Mission Concept Study Final Report*. arXiv:2001.06683 [astro-ph].

Gubner, J. (2018). *"Deformable Mirror Demonstration Mission" by Jennifer Gubner*. Senior Thesis in Applied Physics. Wellesley, MA, Unites States: Wellesley College.

Haughwout, C. A. (2018). *Electronics Development for the Deformable Mirror Demonstration Mission (DeMi)*. Thesis. Cambridge, MA: Massachusetts Institute of Technology.

Heidt, H., Puig-Suari, J., Moore, A., Nakasuka, S., and Twiggs, R. (2000). "CubeSat: A New Generation of Picosatellite for Education and Industry Low-Cost Space Experimentation," in AIAA/USU Conference on Small Satellites.

Kasdin, N. J., Bailey, V., Mennesson, B., Zellem, R., Ygouf, M., Rhodes, J., et al. (2020). "The Nancy Grace Roman Space Telescope Coronagraph Instrument (CGI) Technology Demonstration," in *Space Telescopes and Instrumentation 2020: Optical, Infrared, and Millimeter Wave* (Bellingham, WA: International Society for Optics and Photonics), 11443, 114431U. doi:10.1117/12.2562997

Knapp, M., Seager, S., Demory, B.-O., Krishnamurthy, A., Smith, M. W., Pong, C. M., et al. (2020). Demonstrating High-precision Photometry with a CubeSat: ASTERIA Observations of 55 Cancri e. *AJ* 160, 23. doi:10.3847/1538-3881/ab8bcc

Lesser, D. H., Graves, L., and Walker, C. K. (2019). Active Optical Correctors for Large Inflatable Telescopes. *IEEE Trans. Thz Sci. Technol.* 9, 409–416. doi:10.1109/TTHZ.2019.2918553

Levine, M., Lisman, D., Shaklan, S., Kasting, J., Traub, W., Alexander, J., et al. (2009). *Terrestrial Planet Finder Coronagraph (TPF-C) Flight Baseline Concept*. arXiv:0911.3200 [astro-ph].

Maier, E. R., Douglas, E. S., Kim, D. W., Su, K., Ashcraft, J. N., Breckinridge, J. B., et al. (2020). "Design of the Vacuum High Contrast Imaging Testbed for CDEEP, the Coronagraphic Debris and Exoplanet Exploring Pioneer," in *Space Telescopes and Instrumentation 2020: Optical, Infrared, and Millimeter Wave* (Bellingham, WA: International Society for Optics and Photonics), 11443, 114431Y. doi:10.1117/12.2560878

Marinan, A., and Cahoy, K. (2014). "CubeSat Deformable Mirror Demonstration Mission," in 2014 International Symposium on Optomechatronic Technologies. Seattle, WA: ISOT, 134–138. doi:10.1109/ISOT.2014.40

Marinan, A., Cahoy, K., Merk, J., Belikov, R., and Bendek, E. (2016). "Improving Nanosatellite Imaging with Adaptive Optics," in AIAA/USU Conference on Small Satellites.

Marinan, A. D. (2016). *Improving Nanosatellite Capabilities for Atmospheric Sounding and Characterization*. Cambridge, MA, United States: Thesis, Massachusetts Institute of Technology. Available at: http://dspace.mit.edu/handle/1721.1/105599.

Marx, V. (2017). Microscopy: Hello, Adaptive Optics. *Nat. Methods* 14, 1133–1136. doi:10.1038/nmeth.4508

Mason, J., Baumgart, M., Woods, T., Hegel, D., Rogler, B., Stafford, G., et al. (2016). "MinXSS CubeSat On-Orbit Performance and the First Flight of the Blue Canyon Technologies XACT 3- axis ADCS," In AIAA/USU Conference on Small Satellites.

Mawet, D., Serabyn, E., Liewer, K., Burruss, R., Hickey, J., and Shemo, D. (2010). The Vector Vortex Coronagraph: Laboratory Results and First Light at Palomar Observatory. *ApJ* 709, 53–57. doi:10.1088/0004-637X/709/1/53

Mejia Prada, C., Serabyn, E., and Shi, F. (2019). "High-contrast Imaging Stability Using MEMS Deformable Mirror," in *Techniques and Instrumentation for Detection of Exoplanets IX* (San Diego, CA: International Society for Optics and Photonics), 11117, 1111709. doi:10.1117/12.2525628

Morgan, R. (2019). *Assembly, Integration, and Testing of the Deformable Mirror (DeMi) CubeSat Payload*. Spirit of Lyot. Tokyo, Japan, 1.

Morgan, R. E., Douglas, E. S., Allan, G., Pereira, P. d. V., Gubner, J. N., Haughwout, C., et al. (2021). Optical Calibration and First Light for the Deformable Mirror Demonstration mission CubeSat (DeMi). *JATIS* 7, 024002. doi:10.1117/1.JATIS.7.2.024002

Morgan, R. E., Douglas, E. S., Allan, G. W., Bierden, P., Chakrabarti, S., Cook, T., et al. (2019). MEMS Deformable Mirrors for Space-Based High-Contrast Imaging. *Micromachines* 10, 366. doi:10.3390/mi10060366

Morgan, R. (2020). *Optical Modeling and Validation for the Deformable Mirror Demonstration mission*. Cambridge, MA: Massachusetts Institute of Technology. S.M. Thesis.

Morzinski, K. M., Norton, A. P., Evans, J. W., Reza, L., Severson, S. A., Dillon, D., et al. (2012). "MEMS Practice: from the Lab to the Telescope," in *SPIE MOEMS-MEMS*, 825304. doi:10.1117/12.910964

Perrin, M., Long, J., Douglas, E., Sivaramakrishnan, A., Slocum, C., et al. (2016). *POPPY: Physical Optics Propagation in Python*. Available at: https://ascl.net/1602.018.

Pong, C. (2018). "On-Orbit Performance & Operation of the Attitude & Pointing Control Subsystems on ASTERIA," in AIAA/USU Conference on Small Satellites.

Pueyo, L. A., Stark, C., Juanola-Parramon, R., Zimmerman, N. T., Bolcar, M. R., Roberge, A., et al. (2019). "The LUVOIR Extreme Coronagraph for Living Planetary Systems (ECLIPS) I: Searching and Characterizing Exoplanetary Gems," in *Techniques and Instrumentation for Detection of Exoplanets IX*. Editor S. B. Shaklan (San Diego, United States: SPIE), 3. doi:10.1117/12.2530722

Roberts, L. C., Bryden, G., Traub, W., Unwin, S., Trauger, J., Krist, J., et al. (2013). The Debris Disk Explorer: A Balloon-Borne Coronagraph for Observing Debris Disks. *Proc. SPIE* 8864, 88640A–88640A–88714A. doi:10.1117/12.2025282

Ruane, G., Crill, B., Patterson, K., Prada, C. M., Seo, B.-J., and Siegler, N. (2019). *Decadal Survey Testbed Commissioning Roadmap: Demonstrating Technology for Imaging New Worlds*, 11. Pasadena, CA: Jet Propulsion Laboratory, NASA ExEP Program roadmap.

Sinclair, D., Enright, J., Dzamba, T., and Sears, T. (2015). "Custom Optics vs Modified COTS for Small Spacecraft : The Build vs. Rebuild Decision," in Small Satellite Conference, Logan, Utah.

Sirbu, D., Thomas, S. J., Belikov, R., Lozi, J., Bendek, E., Pluzhnik, E., et al. (2015). "EXCEDE Technology Development IV: Demonstration of Polychromatic Contrast in Vacuum at 1.2 L/D.," in *Techniques and Instrumentation for Detection of Exoplanets VII* (San Diego, CA: International Society for Optics and Photonics), 9605, 96050J. doi:10.1117/.12.2188752

Stapelfeldt, K. R., Brenner, M. P., Warfield, K. R., Dekens, F. G., Belikov, R., Brugarolas, P. B., et al. (2014). Exo-C: a Probe-Scale Space mission to Directly Image and Spectroscopically Characterize Exoplanetary Systems Using an Internal Coronagraph. *Space Telescopes Instrumentation 2014: Opt. Infrared, Millimeter Wave* 9143, 91432K. doi:10.1117/12.2057115

Tyson, R. K., and Frazier, B. W. (2004). Field Guide To Adaptive Optics *(1000 20th Street*. Bellingham, WA 98227-0010 USA: SPIE. doi:10.1117/3.549261

Underwood, C., Pellegrino, S., Lappas, V. J., Bridges, C. P., and Baker, J. (2015). Using CubeSat/micro-Satellite Technology to Demonstrate the Autonomous Assembly of a Reconfigurable Space Telescope (AAReST). *Acta Astronautica* 114, 112–122. doi:10.1016/j.actaastro.2015.04.008

Wahl, D. J., Jian, Y., Bonora, S., Zawadzki, R. J., and Sarunic, M. V. (2015). Wavefront Sensorless Adaptive Optics Fluorescence Biomicroscope for *In Vivo* Retinal Imaging in Mice. *Biomed. Opt. Express* 7, 1–12. doi:10.1364/BOE.7.000001

**Conflict of Interest:** Author JM was employed by Aurora Flight Sciences, a Boeing Company.

The remaining authors declare that the research was conducted in the absence of any commercial or financial relationships that could be construed as a potential conflict of interest.

**Publisher's Note:** All claims expressed in this article are solely those of the authors and do not necessarily represent those of their affiliated organizations, or those of the publisher, the editors and the reviewers. Any product that may be evaluated in this article, or claim that may be made by its manufacturer, is not guaranteed or endorsed by the publisher.